

This document is confidential and is proprietary to the American Chemical Society and its authors. Do not copy or disclose without written permission. If you have received this item in error, notify the sender and delete all copies.

**Engineering Si Anode Interface via Particle Surface Modification: Embedded Organic Carbonates Lead to Enhanced Performance**

Journal:	<i>ACS Applied Energy Materials</i>
Manuscript ID	ae-2021-00374q.R1
Manuscript Type:	Article
Date Submitted by the Author:	n/a
Complete List of Authors:	Jiang, Sisi; Argonne National Laboratory Yang, Zhenzhen; Argonne National Laboratory, Chemical and Engineering Science Liu, Yuzi; Argonne National Laboratory, Center for Nanoscale Materials Johnson, Noah; Argonne National Laboratory Bloom, Ira; Argonne National Laboratory, Zhang, Lu; Argonne National Laboratory, Electrochemical Energy Storage Zhang, Zhengcheng; Argonne National Laboratory,

SCHOLARONE™  
Manuscripts

## Engineering Si Anode Interface *via* Particle Surface Modification: Embedded Organic Carbonates Lead to Enhanced Performance

*Sisi Jiang, Zhenzhen Yang, Yuzi Liu, Noah Johnson, Ira Bloom, Lu Zhang, and Zhengcheng Zhang\**

Dr. S. Jiang, Dr. Z. Yang, Dr. I. Bloom, Dr. L. Zhang and Dr. Z. Zhang  
Chemical Sciences and Engineering Division, Argonne National Laboratory, 9700 S. Cass Ave., Lemont, IL 60439, USA  
\*E-mail: z Zhang@anl.gov

Dr. Y. Liu  
Center for Nano Materials, Argonne National Laboratory, 9700 S. Cass Ave., Lemont, IL 60439, USA

Keywords: surface organic carbonate group, hydrosilylation reaction, Si nanoparticles, solid-electrolyte-interface

### Abstract

Si nanoparticles (SiNPs) are recognized as a promising anode material for next generation high energy lithium-ion batteries. However, due to the more stringent requirements resulting from severe volume change, the solid-electrolyte interphase (SEI) on SiNPs plays a critical role in determining their cycling performance. Engineering the interface for higher stability has become an effective yet challenging approach to accommodate the deterioration of the silicon anode from the repeated lithiation/delithiation process. Herein, we report a novel approach of engineering a covalently bonded organic monolayer of ethylene carbonates onto the surface of the SiNPs that can help form a sturdy SEI. This molecule-level surface modification provides an effective approach to enable high energy density lithium-ion batteries with Si anodes.

### 1. Introduction

While lithium-ion batteries (LIBs) have become widely utilized, new energy storage technology with lower cost, higher energy density, and longer lasting cycle life and calendar life is desired to ultimately enable global electrification and the construction of a self-sustainable society.<sup>1-4</sup> Silicon (Si) has been regarded as one promising candidate for next-

1  
2  
3 generation anodes owing to its high specific capacity (3579 mAhg<sup>-1</sup> for Li<sub>13</sub>Si<sub>4</sub>),  
4 approximately 10 times as high as that of the graphite anodes (372 mAhg<sup>-1</sup>), as well as its  
5 natural abundance and low toxicity.<sup>5-8</sup>  
6  
7  
8  
9

10  
11 However, the application of Si in anodes is hindered by its intrinsic huge volume change  
12 (~300%) during lithiation, leading to Si particle pulverization and continuous fracture and  
13 reformation of the solid-electrolyte-interphase (SEI), a passivation layer formed by the  
14 electrochemical reduction of electrolyte on all low-potential Li-ion battery anodes.<sup>9, 10</sup> One  
15 plausible strategy to crack the Si particle pulverization issue is to reduce the particle size  
16 down to nanoscale. It has been demonstrated that a particle size of <150 nm is a critical  
17 threshold, below which the expansion could be mitigated, and above which fracture and  
18 pulverization take place.<sup>11-14</sup> However, the high surface area (50 m<sup>2</sup>g<sup>-1</sup>) of the nanoparticles  
19 causes a rapid capacity decay of LIB full cell when nano Si is used as an anode, due to the  
20 tremendous surface reactions resulting in large consumption of lithium inventory.<sup>15-17</sup> It has  
21 been well-established that the SEI is an indispensable component in the battery, which  
22 influences cycle life, calendar life and safety of the cell.<sup>18-21</sup> Therefore, tuning the SEI would  
23 also be an effective way to manage the performance of cells containing Si anodes.  
24  
25  
26  
27  
28  
29  
30  
31  
32  
33  
34  
35  
36  
37  
38  
39  
40

41 Given the crucial role of the SEI in a LIB, tremendous effort has been expended to understand  
42 and develop functional electrolytes and additive for Si anodes.<sup>22, 23</sup> Fluoroethylene carbonate  
43 (FEC)<sup>24-26</sup> is so far the most studied and effective additive, along with vinylene carbonate  
44 (VC)<sup>27</sup>, vinyl ethylene carbonate (VEC)<sup>28, 29</sup>, difluoroethylene carbonate (DFEC)<sup>30</sup> silanes<sup>31</sup>,  
45 ethers<sup>32</sup>, carboxylic anhydrides<sup>33</sup>, and organoboron compounds<sup>34</sup>. Although FEC helps extend  
46 the capacity retention of Si anodes, their long-term stability is still far from practical  
47 applications.  
48  
49  
50  
51  
52  
53  
54  
55  
56  
57

1  
2  
3 The chemical composition and hierarchical structure of the SEI layers are not explicitly  
4 understood due to their complexity and the limitation of current analytical techniques.  
5  
6 Recently, Huang *et al.* employed cryogenic transmission electron microscopy (cryo-TEM) to  
7 analyze the SEI at liquid nitrogen temperature under which the chemical and morphological  
8 information of the SEI are well preserved.<sup>35</sup> It is evident that without FEC additive, the SEI  
9 formed on the Si anode generally follows the mosaic model as proposed by Peled *et al.* for  
10 graphite anode<sup>36</sup>, while with FEC additive, the SEI exhibits a layered structure as proposed by  
11 Aubach *et al.*<sup>37,38</sup> Additionally, FEC promotes the formation of an amorphous SEI comprised  
12 of an organic poly(vinylene carbonate) (poly(VC)) deposition on top of the inner inorganic  
13 LiF layer. This structure could accommodate large strain and the volume change of Si during  
14 long-term cycling.  
15  
16  
17  
18  
19  
20  
21  
22  
23  
24  
25  
26  
27  
28

29 To this end, engineering an artificial SEI containing an organic layer on the surface of Si  
30 anode seems an effective approach to tune and strengthen the SEI stability and thus enhance  
31 the cell performance. In this paper, we introduce a new method of attaching an organic layer  
32 of covalently bonded ethylene carbonate (EC) group onto the surface of silicon nanoparticles  
33 (SiNPs) *via* a Pt-catalyzed hydrosilylation reaction. Surface EC groups regulate the SEI  
34 formation and generate an SEI with desired chemical composition and hierarchical  
35 morphology. The new engineered SEI is resilient as evidenced from the improvement of the  
36 electrochemical cell performance and post-cycling analysis. Our research indicates that  
37 surface functionalization is a feasible approach to improve the cycle life of Si anode.  
38  
39  
40  
41  
42  
43  
44  
45  
46  
47  
48  
49

## 50 **2. Experimental Section**

### 51 *2.1 Materials*

52  
53  
54  
55  
56  
57  
58  
59  
60

1  
2  
3 3-(Allyloxy)-1,2-propanediol, diethyl carbonate, potassium carbonate and pristine SiNPs with  
4 average particle size of 50 nm were purchased from Alfa Aesar; allyl methyl carbonate (Allyl-  
5 MC) and platinum divinyltetramethyldisiloxane [Pt(dvs)] (2% in xylene solution solution)  
6 were purchased from Sigma-Aldrich. All chemicals were used as received.  
7  
8  
9  
10

### 11 12 13 14 *2.2 Synthesis of allyl functional precursor Allyl-EC*

15 ((Allyloxy)methyl)-1,3-dioxolan-2-one was synthesized as shown in Figure 1. 1 3-  
16 (Allyloxy)propane-1,2-propanediol (5 g, 3.8 mmol) and diethyl carbonate (15.2 g, 12.9  
17 mmol) and potassium carbonate (0.6 g, 4.3 mmol) were mixed in a two-necked round-  
18 bottomed flask. The mixture was heated up to 120°C with stirring overnight. Once cooled  
19 down to room temperature, the reaction mixture was filtered and then vacuum distilled (10  
20 mmHg) to afford a colorless liquid product (78% yield). <sup>1</sup>H NMR (500 MHz, Chloroform-*d*) δ  
21 5.90 – 5.84 (CH<sub>2</sub>=CH, 2H), 5.30 – 5.20 (CH<sub>2</sub>=CH, 1H), 4.82 (CH<sub>2</sub>, cyclic EC, 2H), 4.52 –  
22 4.39 (CH, cyclic EC, 1H), 4.17 – 4.02 (CH-CH<sub>2</sub>-O, 2H), 3.74 – 3.61 (O-CH<sub>2</sub>-CH, 2H).  
23  
24  
25  
26  
27  
28  
29  
30  
31  
32  
33  
34

### 35 *2.3 Synthesis of Functionalized SiNPs*

36 The 50 nm pristine SiNPs (0.540 g) were dispersed in DI water (5ml) in a PTFE centrifuge  
37 tube to form an evenly distributed suspension. 5 mL of hydrogen fluoride acid (HF) (48 wt %)  
38 was then added to the suspension and the mixture was stirred for 15 min before being diluted  
39 with DI water (20 mL). The SiNPs were then isolated by gravity filtration and the obtained H  
40 terminated SiNPs (H-SiNPs) were dried in a vacuum oven overnight. HF is an extremely  
41 dangerous chemical, and any experiment involving use of HF requires special training prior to  
42 the experiment. PPE includes an anti-flame lab coat, safety goggles with full coverage at eye  
43 area and two layers of gloves (inner layer: nitrile glove; outer layer: butyl rubber glove). The  
44 experiment is performed in a designated area in the fume hood clearly labelled for HF use.  
45  
46  
47  
48  
49  
50  
51  
52  
53  
54  
55  
56  
57 Also, calcium gluconate gel should be accessible in any lab where HF can potentially be used.  
58  
59  
60

1  
2  
3 After the HF etching experiment, all the residue experiment solution is quenched by excessive  
4 amount of  $\text{Ca}(\text{OH})_2$  to get rid of any remaining HF. The introduction of carbonate groups was  
5 carried out in an Argon-purged glove box. H-SiNPs were mixed with allyl agents, Allyl-EC or  
6 Allyl-MC at a molar ratio of 1:2, followed by the addition of 100 ppm Karstedt catalyst  
7 solution. The mixture was stirred at 45 °C overnight before the SiNPs were isolated by  
8 centrifugation (13,000 rpm, 20 min, 3 times).  
9  
10  
11  
12  
13  
14  
15  
16  
17

#### 18 *2.4 Characterization of SiNPs*

19  
20 Fourier-transform infrared (FTIR) spectra were acquired on a Thermo Scientific Nicolet iS5  
21 spectrometer using attenuated total reflection model placed in an Argon-filled glove box.  
22  
23 Thermogravimetric analysis (TGA) was conducted with a heating rate of 20°C/min from 30°C  
24 to 800°C with Argon purge using the NETZSCH STA 449 F3 Jupiter for simultaneous  
25 thermogravimetry-differential scanning calorimetry (STA/TG-DSC). X-ray photoelectron  
26 spectroscopy of the SiNPs and electrodes were performed in a PHI 5000 XPS VersaProbe II  
27 system from Physical Electronics. The system is attached to the Ar-atmosphere glovebox and  
28 the samples were inserted into the XPS analysis chamber through the glovebox without  
29 exposure to air. The spectra were obtained using an Al  $K\alpha$  radiation ( $h\nu = 1486.6$  eV) beam  
30 (100  $\mu\text{m}$ , 25 W), with  $\text{Ar}^+$  and electron beam sample neutralization, in Fixed Analyzer  
31 Transmission mode. The base pressure is typically  $\sim 2 \times 10^{-8}$  torr or lower in the analysis  
32 chamber. To compensate for the effects of surface charging, all core-level spectra were  
33 referenced to the  $\text{C}_{1s}$  hydrocarbon peak at 284.8 eV. Shirley background subtraction and  
34 fitting to multiple Gaussian-Lorentz peaks were performed on all spectra using the Multipack  
35 software from Physical Electronics. The morphology of SiNPs were analyzed with an JEOL  
36 JEM-2100F transmission electron microscopy (TEM).  
37  
38  
39  
40  
41  
42  
43  
44  
45  
46  
47  
48  
49  
50  
51  
52  
53  
54  
55  
56

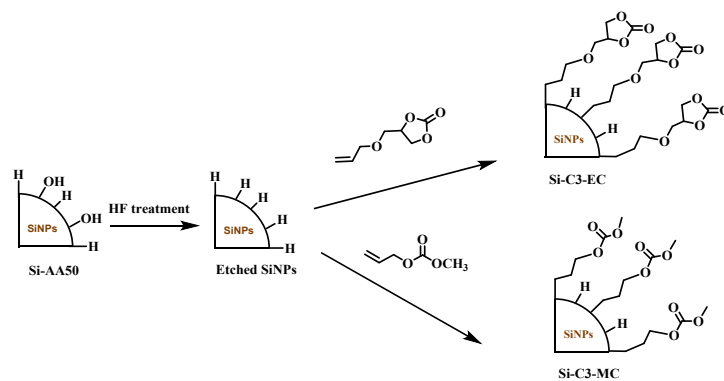
#### 57 *2.5 Electrochemical Measurement and Post-Analysis*

1  
2  
3 To prepare the silicon anode laminations, SiNPs (70%), poly acrylic acid (PAA) binder (20%)  
4 and Timcal C45 (10%) were thoroughly mixed in DI water with a weight ratio of 7:2:1. The  
5 resulting slurry was then cast into a 50  $\mu\text{m}$  laminate using a doctor blade on a Cu current  
6 collector, which was dried under vacuum at 80°C overnight. The cured electrode was punched  
7 into disks of 1.54  $\text{cm}^2$  with a loading of 1-1.2  $\text{mg}/\text{cm}^2$  and further dried at 130 °C in vacuum  
8 for 16 hours. The dried electrodes were then assembled into 2032-coin cells against either Li  
9 metal (half-cells) or lithium nickel manganese cobalt oxide ( $\text{LiNi}_{0.6}\text{Mn}_{0.2}\text{Co}_{0.2}\text{O}_2$ , from the  
10 Argonne Cell Analysis, Modeling, and Prototyping (CAMP) facilities, the loading of the  
11 NMC622 cathode is 9.35  $\text{mg}/\text{cm}^2$ . The n/p ratio is approximately 1.2. ) using Celgard 2325 as  
12 the separator, and Gen 2 (1.2 M  $\text{LiPF}_6$  in EC:EMC 1:2 by weight) electrolyte with 10 wt%  
13 FEC as the electrolyte. Electrochemical impedance spectra of the coin cells after 1st cycle at  
14 C/20 were recorded versus an open-circuit voltage in the frequency range between 1 MHz to  
15 0.1 Hz on a Solartron analytical 1400 Cell Test System. The cycled coin cells were  
16 disassembled in the argon-filled glovebox, and the composite electrodes were rinsed  
17 thoroughly with anhydrous dimethyl carbonate (DMC) and were dried in a vacuum oven. The  
18 morphologies and the elemental mapping of the cycled electrodes were examined with JEOL  
19 JCM-6000Plus scanning electron microscopy (SEM) equipped with MP-05030EDK energy-  
20 dispersive X-ray spectroscopy (EDX), TEM and XPS  
21  
22  
23  
24  
25  
26  
27  
28  
29  
30  
31  
32  
33  
34  
35  
36  
37  
38  
39  
40  
41  
42  
43

### 44 3. Results and Discussion

45  
46 Attaching an artificial SEI onto the surface of SiNPs is not straightforward; fortunately, the  
47 native layer of  $\text{SiO}_x$  on the surface of SiNPs can be etched with HF aqueous solution,  
48 converting  $-\text{SiO}_x$  to  $-\text{SiH}_x$  which can be used as a reaction platform for the next step of the  
49 reaction. The  $-\text{SiH}_x$ -terminated particles (H-SiNPs) then undergo a Pt-catalyzed  
50 hydrosilylation reaction with a reagent with a desired functional group, forming a covalently  
51 bonded organic layer. <sup>[19,20]</sup> **Figure 1** shows the synthesis procedure. Two reagents with the  
52  
53  
54  
55  
56  
57  
58  
59  
60

1  
2  
3 cyclic carbonate group 4-((allyloxy)methyl)-1,3-dioxolan-2-one (Allyl-EC) and linear  
4 carbonate group allyl methyl carbonate (Allyl-MC)) were selected for the hydrosilylation  
5 reaction and SiNPs with cyclic carbonate groups (EC-SiNPs) and linear methyl carbonate  
6 groups (MC-SiNPs) were synthesized.  
7  
8  
9  
10



24 **Figure 1.** Synthesis of SiNPs particles functionalized with surface carbonate groups.  
25

26  
27 **Figure 2a** shows the FT-IR spectra of the surface functionalized SiNPs. After HF treatment,  
28 the characteristic peak at  $2100\text{ cm}^{-1}$  for Si-H group increased and the OSi-H peak at  $2300\text{ cm}^{-1}$   
29 nearly disappeared, indicating the successful conversion of surface SiO<sub>x</sub> and OSi-H groups to  
30 the SiH<sub>x</sub> functionality. After the hydrosilylation reaction, the characteristic IR peaks from the  
31 attached surface group appeared, including the stretching mode of carbonyl ( $\nu\text{C}=\text{O}$ ) at  $1725\text{ cm}^{-1}$   
32  $\nu\text{C}-\text{H}$  at  $2900\text{--}2800\text{ cm}^{-1}$  and the bending mode of  $\delta\text{C}-\text{H}$  at  $1500\text{ cm}^{-1}$  and  $\delta\text{Si}-\text{CH}_2$  at  
33  $1260\text{ cm}^{-1}$  (the expanded IR spectra on the right). The  $\nu\text{C}-\text{O}$  stretching vibration peak at  $1000\text{ cm}^{-1}$   
34 is overlapped with the  $\nu\text{Si}-\text{O}-\text{Si}$  which was formed by the reaction of surface Si-H with  
35 trace amount of moisture in the reaction solvent.<sup>39</sup> From HRTEM imaging, the crystalline  
36 structure of the bulk Si particles are well preserved, while a striking difference is seen on the  
37 surface: a thin and dense SiO<sub>x</sub> layer was observed for the pristine particle, whereas the  
38 functionalized particle has a loose and amorphous organic layer with a thickness  $\sim 2.8\text{ nm}$ , as  
39 shown in **Figure 2b**.  
40  
41  
42  
43  
44  
45  
46  
47  
48  
49  
50  
51  
52  
53  
54  
55  
56  
57  
58  
59  
60

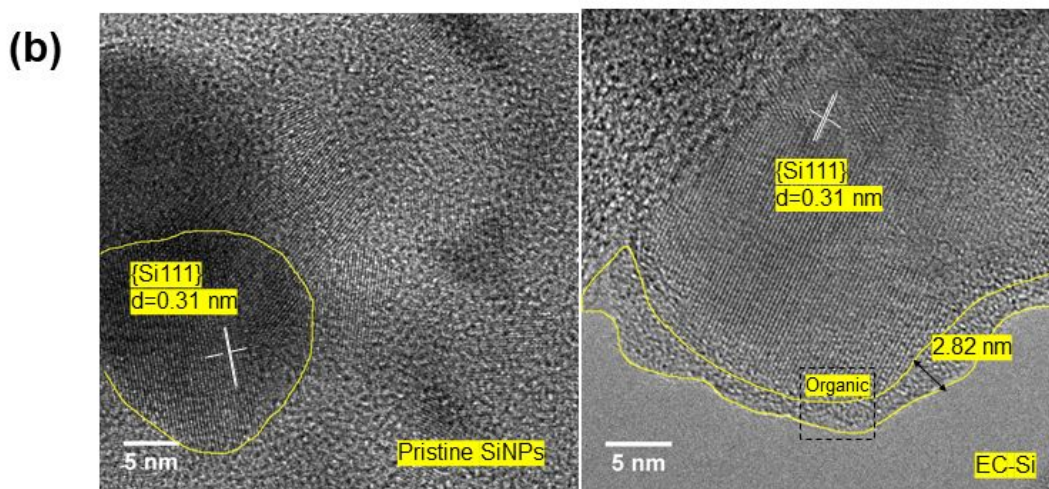
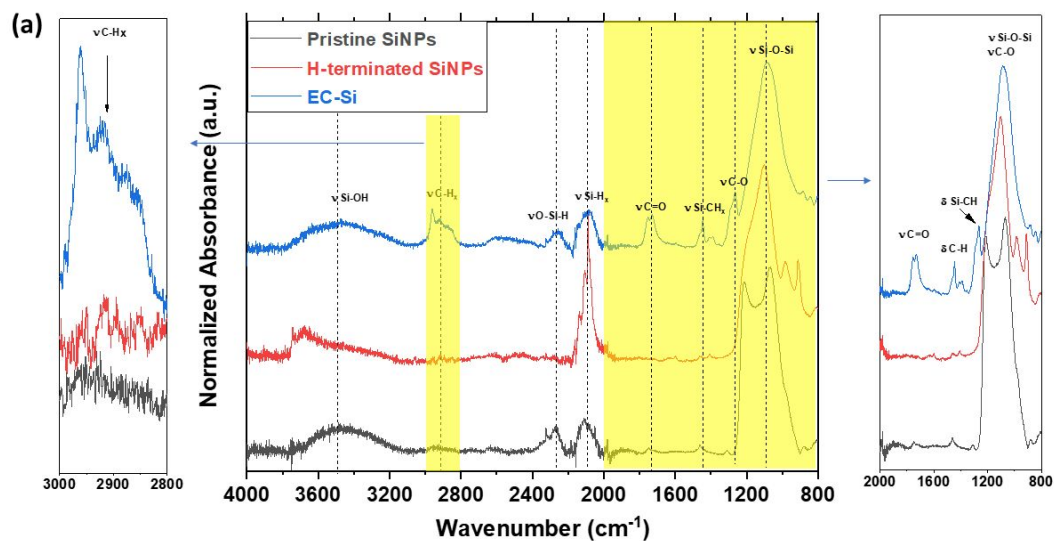


**Figure 2.** Characterization of the surface group on the synthesized EC-SiNPs. (a) ATR-FTIR whole spectra (center) and expanded wavenumber range from 2800-3000  $\text{cm}^{-1}$  (left) and 800-2000  $\text{cm}^{-1}$  (right) and (b) TEM micrographs of the SiNPs before (left) and after (right) surface functionalization.

1  
2  
3 **Figure 3a** shows the voltage profiles of the SiNPs/Li half cells cycled between 1.5 – 0.01 V.  
4  
5 The first lithiation process for both EC-functionalized SiNPs and pristine Si anode resemble  
6  
7 each other with an abrupt voltage drop from open circuit voltage to around 0.1 V followed by  
8  
9 a flat plateau that represents the transition from crystalline phase to amorphous phase.  
10  
11 Notable differences were observed, however, on the differential capacity profiles in **Figure 3b**,  
12  
13 where the EC-SiNP anode shows a sharp reduction peak at 1.6 V (*vs* Li<sup>+</sup>/Li thereafter),  
14  
15 contrasting with the pristine anode, which is dominated by FEC reduction (1.3 V).<sup>40</sup>  
16  
17 This indicates that the SEI formation for the EC-Si anode took a different path where the  
18  
19 surface EC group preferably gets reduced, forming a completely different SEI in terms of  
20  
21 chemical composition and structure. Two adjacent EC groups on the Si surface underwent a  
22  
23 two-electron reduction process generating a SEI layer containing an inorganic lithium  
24  
25 ethylene dicarbonate (LiEDC) outer layer covalently bonded to an organic polyolefin-rich  
26  
27 inner layer. Detailed XPS analysis in the post-test analysis section further confirmed the  
28  
29 unique surface group regulated SEI.  
30  
31  
32  
33  
34

35 The efficacy of the surface functional groups was demonstrated in the formation cycles (C/20)  
36  
37 and repeated cycling (C/3). Interestingly, we found that at the beginning of C/3 cycling, FCE  
38  
39 (98.0%) of EC-SiNP anode was lower than that of pristine anode (over 99.0wt%) (**Figure 3c**).  
40  
41 This is because that surface carbonate interacts differently with electrolyte other than pristine  
42  
43 anode surface and therefore it might consume more Li. Then after approximately 20 cycles,  
44  
45 the trend in FCE reverse where the FCE of pristine anode gradually declines to 97% and that  
46  
47 of EC-SiNP anode continues to increase to over 99.0%, which indicates that the SEI formed  
48  
49 on EC-SiNP anode surface is more robust and has less impedance build-up as is revealed by  
50  
51 the EIS data (**Figure S4** in supporting information). Accordingly, the cycling retention of EC-  
52  
53 SiNP anode (75%) is higher than pristine anode (60%) at 100 cycles. Additionally, the SEI  
54  
55 and its impact on the cell performance closely relates to the chemical structure of the surface  
56  
57  
58  
59  
60

1  
2  
3 functional groups. As shown in Figure 3c, a linear carbonate attached SiNPs (MC-Si) was  
4 synthesized in the same way. Although very similar in performance with the EC-Si electrode  
5 during the initial 20 cycles, the capacity of the MC-Si cell gradually decayed afterwards, with  
6 only 56.6% capacity retention after 100 cycles. It is speculated that the linear carbonate group  
7 on the Si surface is incapable of forming the well-designed SEI which is seen in the EC-Si  
8 anode with an inorganic-rich outer layer. This result is in good agreement with the EC/linear  
9 carbonate/LiPF<sub>6</sub>-based electrolytes, where only the cyclic EC participates in the SEI  
10 formation, rather than the linear carbonates.<sup>41</sup>  
11  
12  
13  
14  
15  
16  
17  
18  
19  
20  
21

22 Given the unlimited lithium inventory, the improved performance of the Si anode in the half  
23 cells rarely translates to the same performance in the full cells. To evaluate its performance in  
24 the full cell, EC-Si anode is balanced with a state-of-the-art nickel-rich NMC622  
25 (LiNi<sub>0.6</sub>Mn<sub>0.2</sub>Co<sub>0.2</sub>O<sub>2</sub>) cathode. The NMC622/EC-Si cells underwent a formation process with  
26 three C/20 cycles followed by 97 C/3 cycles and another three C/20 cycles for capacity check.  
27  
28 **Figure 3d** summarizes the cycling data. As expected, while both pristine and EC-SiNPs cells  
29 show nearly identical initial capacities, EC-SiNPs outperforms over the prolonged cycling  
30 course with an improved capacity retention of 74% compared to the 63% of the pristine SiNPs  
31 cell.  
32  
33  
34  
35  
36  
37  
38  
39  
40  
41  
42  
43  
44  
45  
46  
47  
48  
49  
50  
51  
52  
53  
54  
55  
56  
57  
58  
59  
60

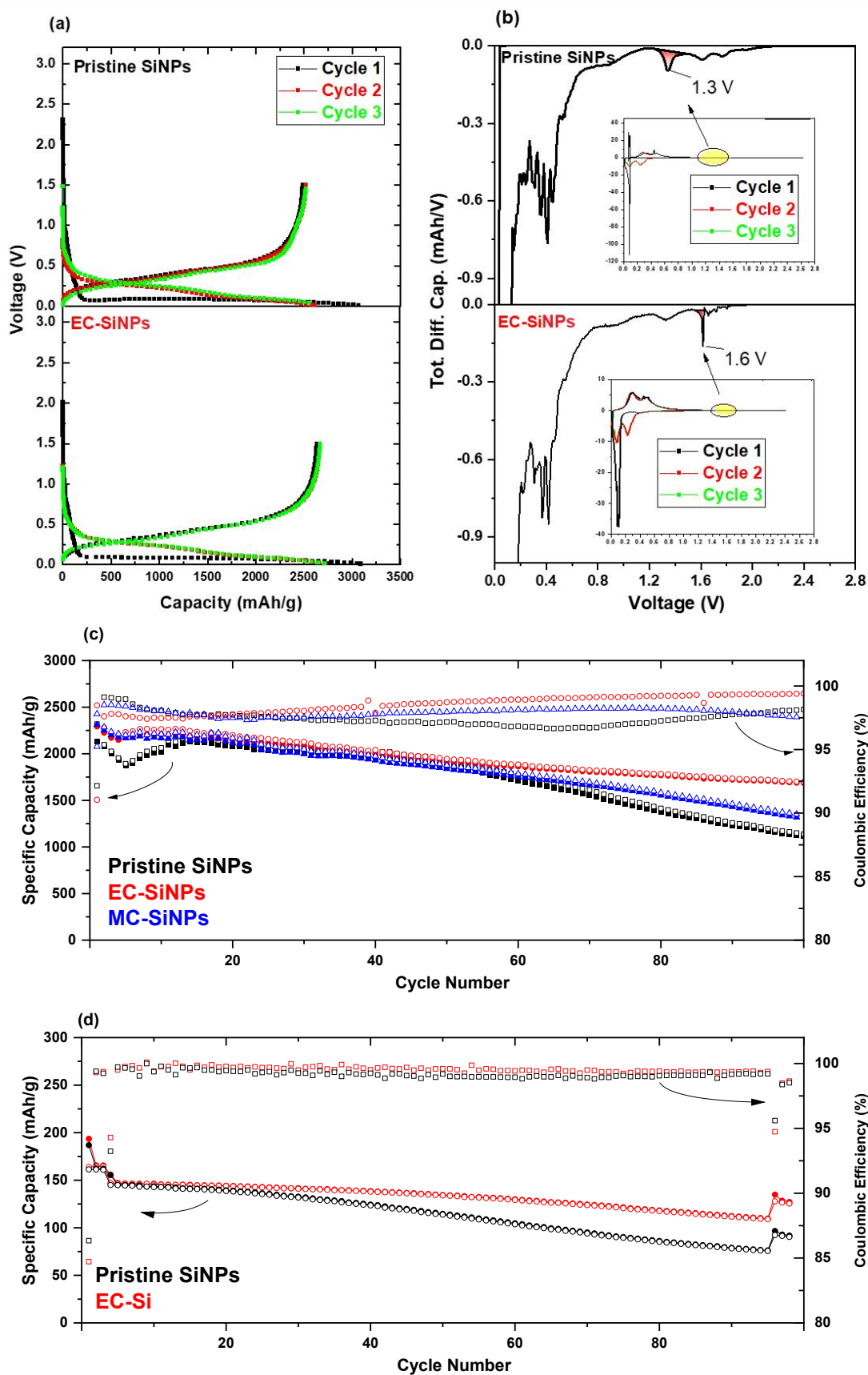
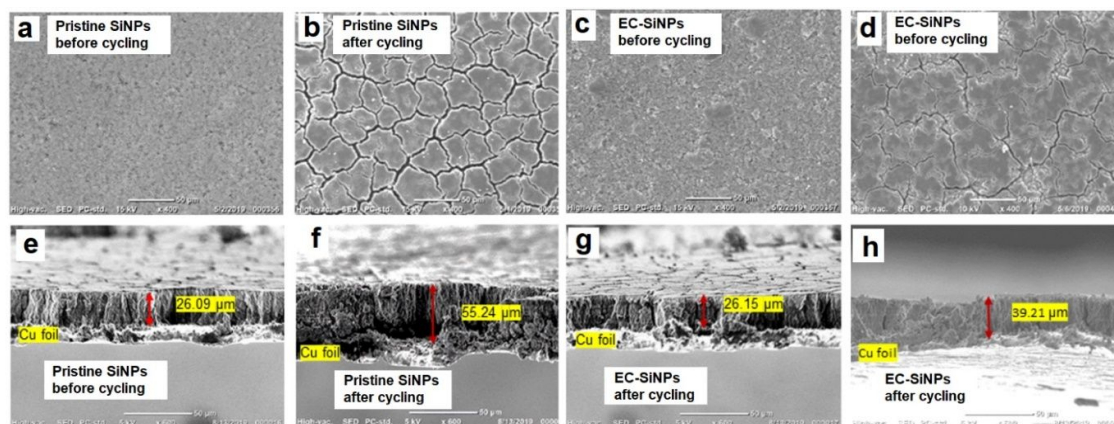


**Figure 3.** Electrochemical performance of surface functionalized EC-SiNPs in comparison with pristine Si anode. (a) Voltage-capacity profiles, (b) differential capacity ( $dQ/dV$ ) profiles for formation cycles, (c) capacity retention and Coulombic efficiency of SiNPs/Li half cells and (d) cycling performance of Si/NMC622 full cells.

The determinant role of surface EC-group regulated SEI can also be visualized by the electrode morphology and its chemical composition. SEM images of the pristine and surface functionalized Si electrodes before and after 100 cycles are shown in **Figure 4**. Before cycling, both electrodes resemble each other with uniform surface morphology (**Figure 4a, 4c**). However, after cycling the pristine SiNPs electrode showed large and deep cracks while EC-SiNPs electrode showed minimal cracking (**Figure 4b, 4d**). The thickness of the cycled electrodes at the fully delithiated state were analyzed by the cross-sectional SEM imaging. The pristine SiNPs electrode increases in thickness more than 100% (from 26 to 55  $\mu\text{m}$ ), caused by the accumulation of electrolyte decomposition products. In contrast, the EC-SiNPs electrode only increases 50% (from 26 to 39  $\mu\text{m}$ ) ascribed to the thinner SEI and more stabilized interface which suppressed the continuous decomposition of electrolyte.



1  
2  
3 **Figure 4.** Morphology of cycled SiNPs anode. (a, b) SEM images of pristine Si anode before  
4 and after cycling, (c, d) SEM of cross-section of pristine SiNPs before and after cycling, (e, f)  
5 SEM images of EC-Si anode before and after cycling, and (g, h) SEM images of cross-section  
6 of EC-SiNPs anode before and after cycling.  
7  
8  
9  
10

11  
12  
13 The SEI composition and chemical distribution were examined by XPS. Before cycling, the  
14 EC-Si anode surface was covered by organic carbonate groups covalently bonded to the  
15 surface, i.e. 284.8 eV for C-C bond, 285.8 eV for carbonate C-O bond and 288.9 eV for  
16 carbonate C=O bond (**Figure 5a**, top), and no C-O or C=O bond were found on the surface of  
17 pristine Si anode as shown in the C<sub>1s</sub> XPS spectra (**Figures 5a**, bottom).<sup>42</sup> After 100 cycles,  
18 dramatic change was observed for the cycled pristine anode surface and heavy deposition by  
19 decomposed species of electrolyte solvent and FEC additive as evidenced by the large peaks  
20 of C-O and C=O species (**Figure 5b**, bottom), which are absent before cycling.<sup>43, 44</sup> In  
21 contrast, the surface species on the cycled EC-SiNPs anode resembles the original state with  
22 only a slight decrease in concentration (**Figure 5b**, top), indicating the attached EC groups  
23 stabilize the interface and suppress the SEI growth with cycling. F<sub>1s</sub> XPS data further  
24 confirmed the interfacial stabilization by EC groups. Large amounts of inorganic species from  
25 LiPF<sub>6</sub> decomposition, including LiF and Li<sub>x</sub>PO<sub>y</sub>F<sub>z</sub>, observed in the cycled pristine Si anode  
26 (**Figure 5c**, bottom) were significantly suppressed in the EC-SiNPs anode (**Figure 5c**, top).<sup>43</sup>  
27  
28 Based on this results, a possible SEI formation mechanism was proposed. Instead of the EC  
29 solvent molecules, the attached ethylene carbonate group on the Si surface preferably  
30 participates in the two-electron reduction reaction of two adjacent EC groups on the Si surface  
31 forming a unique SEI with an inner elastomeric polyethylene covalently bonded to the Si  
32 anode and an outer inorganic analog of LEDC. XPS analysis results provide further proof that  
33 the surface carbonate group is favorable to Si anode. The unique organic-rich SEI can  
34  
35  
36  
37  
38  
39  
40  
41  
42  
43  
44  
45  
46  
47  
48  
49  
50  
51  
52  
53  
54  
55  
56  
57  
58  
59  
60

accommodate the volume change of Si and stabilize the interface with the electrolyte. These results are consistent with the electrochemical performance.

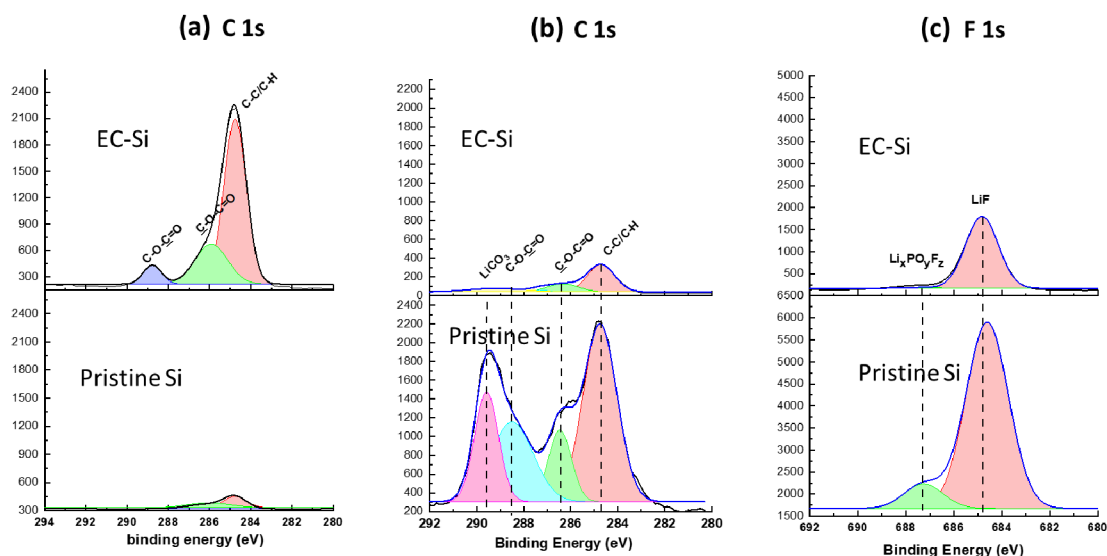


**Figure 5.** XPS spectra of EC-SiNPs and pristine Si electrodes. (a) C<sub>1s</sub> XPS spectra of EC-SiNPs (top) and pristine Si electrode (bottom) before cycling; (b) C<sub>1s</sub> XPS spectra of EC-SiNPs (top) and pristine Si electrode (bottom) after 100 cycles; (c) F<sub>1s</sub> XPS spectra of EC-SiNPs (top) and pristine Si electrode (bottom) after 100 cycles.

#### 4. Conclusions

In this paper, we report a new Si anode material with a cyclic carbonate group attached to the surface via a Pt-catalyzed hydrosilylation reaction. The organic carbonate groups help stabilize the Si anode interface and suppress the parasitic reactions of the Li<sub>x</sub>Si with electrolyte as evidenced by its improved initial capacity and capacity retention in both Li/Si half cells and Si/NMC622 full cells compared with the non-functionalized one. Post-test analysis revealed that EC-SiNPs doesn't suffer from electrode thickness growth and affords a much thinner and more regulated SEI layer, which stabilizes the interface and helps accommodate the volume expansion/contraction of the SiNPs during cycling. The concept of attaching SEI-formation functional groups on the Si particle level via organic chemistry offers

1  
2  
3 a promising avenue to overcome the challenges associated with the Si anodes.  
4  
5

### 6 7 **Supporting Information**

8  
9 <sup>1</sup>H-NMR spectrum of EC-SiNPs and its synthesis scheme; TGA thermogram of the EC-SiNPs  
10  
11 particles; TEM images of the cycled silicon anodes; Nyquist plots of cycled Si/NMC622 full  
12  
13 cells; SEM image and EDS elemental mapping for Si, O, F, P and their chemical composition.  
14  
15

### 16 17 **Acknowledgements**

18  
19 This research is supported by the U.S. Department of Energy (DOE), Vehicle Technologies  
20  
21 Office. Use of the Center for Nanoscale Materials for the SEM/EDS and TEM analysis was  
22  
23 supported by the U.S. Department of Energy, Office of Science, and Office of Basic Energy  
24  
25 Sciences. Argonne National Laboratory is operated by UChicago Argonne, LLC for DOE  
26  
27 Office of Science under contract number DE-AC02-06CH11357.  
28  
29  
30  
31  
32  
33  
34  
35  
36  
37  
38  
39  
40  
41  
42  
43  
44  
45  
46  
47  
48  
49  
50  
51  
52  
53  
54  
55  
56  
57  
58  
59  
60

## Reference

- 1 (1) Armand, M.; Tarascon, J. M., Building better batteries. *nature* **2008**, *451* (7179), 652-657.
- 2 (2) Scrosati, B.; Hassoun, J.; Sun, Y.-K., Lithium-ion batteries. A look into the future. *Energy & Environmental Science* **2011**, *4* (9), 3287-3295.
- 3 (3) Schmich, R.; Wagner, R.; Hörpel, G.; Placke, T.; Winter, M., Performance and cost of materials for lithium-based rechargeable automotive batteries. *Nature Energy* **2018**, *3* (4), 267-278.
- 4 (4) Manthiram, A., A reflection on lithium-ion battery cathode chemistry. *Nature Communications* **2020**, *11* (1), 1550.
- 5 (5) Magasinski, A.; Dixon, P.; Hertzberg, B.; Kvit, A.; Ayala, J.; Yushin, G., High-performance lithium-ion anodes using a hierarchical bottom-up approach. *Nature materials* **2010**, *9* (4), 353-358.
- 6 (6) Szczech, J. R.; Jin, S., Nanostructured silicon for high capacity lithium battery anodes. *Energy & Environmental Science* **2011**, *4* (1), 56-72.
- 7 (7) Wu, H.; Cui, Y., Designing nanostructured Si anodes for high energy lithium ion batteries. *Nano today* **2012**, *7* (5), 414-429.
- 8 (8) Feng, K.; Li, M.; Liu, W.; Kashkooli, A. G.; Xiao, X.; Cai, M.; Chen, Z., Silicon - based anodes for lithium - ion batteries: From fundamentals to practical applications. *Small* **2018**, *14* (8), 1702737.
- 9 (9) Chae, S.; Ko, M.; Kim, K.; Ahn, K.; Cho, J., Confronting Issues of the Practical Implementation of Si Anode in High-Energy Lithium-Ion Batteries. *Joule* **2017**, *1* (1), 47-60.
- 10 (10) Chae, S.; Choi, S.-H.; Kim, N.; Sung, J.; Cho, J., Integration of Graphite and Silicon Anodes for the Commercialization of High-Energy Lithium-Ion Batteries. *Angewandte Chemie International Edition* **2020**, *59* (1), 110-135.
- 11 (11) Kim, H.; Seo, M.; Park, M.-H.; Cho, J., A Critical Size of Silicon Nano-Anodes for Lithium Rechargeable Batteries. *Angewandte Chemie International Edition* **2010**, *49* (12), 2146-2149.
- 12 (12) Hou, J.; Qu, S.; Yang, M.; Zhang, J., Materials and electrode engineering of high capacity anodes in lithium ion batteries. *Journal of Power Sources* **2020**, *450*, 227697.
- 13 (13) Chan, C. K.; Peng, H.; Liu, G.; McIlwrath, K.; Zhang, X. F.; Huggins, R. A.; Cui, Y., High-performance lithium battery anodes using silicon nanowires. *Nature Nanotechnology* **2008**, *3* (1), 31-35.
- 14 (14) Wu, H.; Yu, G.; Pan, L.; Liu, N.; McDowell, M. T.; Bao, Z.; Cui, Y., Stable Li-ion battery anodes by in-situ polymerization of conducting hydrogel to conformally coat silicon nanoparticles. *Nature communications* **2013**, *4* (1), 1-6.
- 15 (15) Zhang, Y.; Du, N.; Yang, D., Designing superior solid electrolyte interfaces on silicon anodes for high-performance lithium-ion batteries. *Nanoscale* **2019**, *11* (41), 19086-19104.
- 16 (16) Eom, K.; Joshi, T.; Bordes, A.; Do, I.; Fuller, T. F., The design of a Li-ion full cell battery using a nano silicon and nano multi-layer graphene composite anode. *Journal of Power Sources* **2014**, *249*, 118-124.
- 17 (17) Jin, Y.; Li, S.; Kushima, A.; Zheng, X.; Sun, Y.; Xie, J.; Sun, J.; Xue, W.; Zhou, G.; Wu, J.; Shi, F.; Zhang, R.; Zhu, Z.; So, K.; Cui, Y.; Li, J., Self-healing SEI enables full-cell cycling of a silicon-majority anode with a coulombic efficiency exceeding 99.9%. *Energy & Environmental Science* **2017**, *10* (2), 580-592.
- 18 (18) An, S. J.; Li, J.; Daniel, C.; Mohanty, D.; Nagpure, S.; Wood, D. L., The state of understanding of the lithium-ion-battery graphite solid electrolyte interphase (SEI) and its relationship to formation cycling. *Carbon* **2016**, *105*, 52-76.

- 1  
2  
3 (19) Zhang, S.; Ding, M. S.; Xu, K.; Allen, J.; Jow, T. R., Understanding solid electrolyte  
4 interface film formation on graphite electrodes. *Electrochemical and Solid State Letters* **2001**,  
5 *4* (12), A206.
- 6 (20) Xu, K., Electrolytes and interphases in Li-ion batteries and beyond. *Chemical reviews*  
7 **2014**, *114* (23), 11503-11618.
- 8 (21) Shen, B. H.; Veith, G. M.; Tenhaeff, W. E., Silicon surface tethered polymer as  
9 artificial solid electrolyte interface. *Scientific reports* **2018**, *8* (1), 1-11.
- 10 (22) Xu, Z.; Yang, J.; Li, H.; Nuli, Y.; Wang, J., Electrolytes for advanced lithium ion  
11 batteries using silicon-based anodes. *J. Mater. Chem. A* **2019**, *7* (16), 9432-9446.
- 12 (23) Kennedy, T.; Brandon, M.; Laffir, F.; Ryan, K. M., Understanding the influence of  
13 electrolyte additives on the electrochemical performance and morphology evolution of silicon  
14 nanowire based lithium-ion battery anodes. *Journal of Power Sources* **2017**, *359*, 601-610.
- 15 (24) Ma, L.; Xia, J.; Xia, X.; Dahn, J., The impact of vinylene carbonate, fluoroethylene  
16 carbonate and vinyl ethylene carbonate electrolyte additives on electrode/electrolyte reactivity  
17 studied using accelerating rate calorimetry. *Journal of the Electrochemical Society* **2014**, *161*  
18 (10), A1495.
- 19 (25) Schroder, K.; Alvarado, J.; Yersak, T. A.; Li, J.; Dudney, N.; Webb, L. J.; Meng,  
20 Y. S.; Stevenson, K. J., The effect of fluoroethylene carbonate as an additive on the solid  
21 electrolyte interphase on silicon lithium-ion electrodes. *Chemistry of Materials* **2015**, *27* (16),  
22 5531-5542.
- 23 (26) Lindgren, F.; Xu, C.; Niedzicki, L.; Marcinek, M.; Gustafsson, T. r.; Björefors, F.;  
24 Edström, K.; Younesi, R., SEI formation and interfacial stability of a Si electrode in a LiTDI-  
25 salt based electrolyte with FEC and VC additives for Li-ion batteries. *ACS applied materials*  
26 *& interfaces* **2016**, *8* (24), 15758-15766.
- 27 (27) Chen, L.; Wang, K.; Xie, X.; Xie, J., Effect of vinylene carbonate (VC) as electrolyte  
28 additive on electrochemical performance of Si film anode for lithium ion batteries. *Journal of*  
29 *Power Sources* **2007**, *174* (2), 538-543.
- 30 (28) Shim, E.-G.; Nam, T.-H.; Kim, J.-G.; Kim, H.-S.; Moon, S.-I., Effect of vinyl acetate  
31 plus vinylene carbonate and vinyl ethylene carbonate plus biphenyl as electrolyte additives on  
32 the electrochemical performance of Li-ion batteries. *Electrochimica acta* **2007**, *53* (2), 650-  
33 656.
- 34 (29) Yang, Y.; Xiong, J.; Lai, S.; Zhou, R.; Zhao, M.; Geng, H.; Zhang, Y.; Fang, Y.;  
35 Li, C.; Zhao, J., Vinyl ethylene carbonate as an effective SEI-forming additive in carbonate-  
36 based electrolyte for lithium-metal anodes. *ACS applied materials & interfaces* **2019**, *11* (6),  
37 6118-6125.
- 38 (30) Xia, J.; Petibon, R.; Xiao, A.; Lamanna, W.; Dahn, J., Some fluorinated carbonates  
39 as electrolyte additives for Li (Ni<sub>0.4</sub>Mn<sub>0.4</sub>Co<sub>0.2</sub>) O<sub>2</sub>/graphite pouch cells. *Journal of The*  
40 *Electrochemical Society* **2016**, *163* (8), A1637.
- 41 (31) Ryu, Y.-G.; Lee, S.; Mah, S.; Lee, D. J.; Kwon, K.; Hwang, S.; Doo, S.,  
42 Electrochemical behaviors of silicon electrode in lithium salt solution containing alkoxy  
43 silane additives. *J. Electrochem. Soc* **2008**, *155* (8), A583-A589.
- 44 (32) Noguchi, T.; Hasegawa, T.; Yamauchi, H.; Yamazaki, I.; Utsugi, K., Effect of Using  
45 Fluorinated Ether and Sulfone as Electrolyte Solvents for Lithium Ion Batteries with Lithium-  
46 Rich Layered Cathodes and Silicon Oxide Anodes. **2017**, *80* (10), 291-303.
- 47 (33) Yan, Y.; Yin, Y.-X.; Xin, S.; Su, J.; Guo, Y.-G.; Wan, L.-J., High-safety lithium-  
48 sulfur battery with prelithiated Si/C anode and ionic liquid electrolyte. *Electrochimica Acta*  
49 **2013**, *91*, 58-61.
- 50 (34) Lee, S. J.; Han, J.-G.; Lee, Y.; Jeong, M.-H.; Shin, W. C.; Ue, M.; Choi, N.-S., A  
51 bi-functional lithium difluoro(oxalato)borate additive for lithium cobalt oxide/lithium nickel  
52 manganese cobalt oxide cathodes and silicon/graphite anodes in lithium-ion batteries at  
53 elevated temperatures. *Electrochim. Acta* **2014**, *137*, 1-8.
- 54  
55  
56  
57  
58  
59  
60

- 1  
2  
3 (35) Huang, W.; Wang, J.; Braun, M. R.; Zhang, Z.; Li, Y.; Boyle, D. T.; McIntyre, P.  
4 C.; Cui, Y., Dynamic Structure and Chemistry of the Silicon Solid-Electrolyte Interphase  
5 Visualized by Cryogenic Electron Microscopy. *Matter* **2019**, *1* (5), 1232-1245.
- 6 (36) Peled, E.; Golodnitsky, D.; Ardel, G., Advanced Model for Solid Electrolyte  
7 Interphase Electrodes in Liquid and Polymer Electrolytes. *Journal of The Electrochemical*  
8 *Society* **1997**, *144* (8), L208-L210.
- 9 (37) Aurbach, D.; Moshkovich, M.; Cohen, Y.; Schechter, A., The study of surface film  
10 formation on noble-metal electrodes in alkyl carbonates/Li salt solutions, using simultaneous  
11 in situ AFM, EQCM, FTIR, and EIS. *Langmuir* **1999**, *15* (8), 2947-2960.
- 12 (38) Aurbach, D., Review of selected electrode–solution interactions which determine the  
13 performance of Li and Li ion batteries. *Journal of Power Sources* **2000**, *89* (2), 206-218.
- 14 (39) Smith, A. L., Infrared spectra-structure correlations for organosilicon compounds.  
15 *Spectrochimica Acta* **1960**, *16* (1), 87-105.
- 16 (40) Shobukawa, H.; Alvarado, J.; Yang, Y.; Meng, Y. S., Electrochemical performance  
17 and interfacial investigation on Si composite anode for lithium ion batteries in full cell.  
18 *Journal of Power Sources* **2017**, *359*, 173-181.
- 19 (41) Xu, K., Nonaqueous Liquid Electrolytes for Lithium-Based Rechargeable Batteries.  
20 *Chemical Reviews* **2004**, *104* (10), 4303-4418.
- 21 (42) Michan, A. L.; Parimalam, B. S.; Leskes, M.; Kerber, R. N.; Yoon, T.; Grey, C. P.;  
22 Lucht, B. L., Fluoroethylene Carbonate and Vinylene Carbonate Reduction: Understanding  
23 Lithium-Ion Battery Electrolyte Additives and Solid Electrolyte Interphase Formation.  
24 *Chemistry of Materials* **2016**, *28* (22), 8149-8159.
- 25 (43) Nguyen, C. C.; Yoon, T.; Seo, D. M.; Guduru, P.; Lucht, B. L., Systematic  
26 Investigation of Binders for Silicon Anodes: Interactions of Binder with Silicon Particles and  
27 Electrolytes and Effects of Binders on Solid Electrolyte Interphase Formation. *ACS Applied*  
28 *Materials & Interfaces* **2016**, *8* (19), 12211-12220.
- 29 (44) Chen, J.; Fan, X.; Li, Q.; Yang, H.; Khoshi, M. R.; Xu, Y.; Hwang, S.; Chen, L.;  
30 Ji, X.; Yang, C.; He, H.; Wang, C.; Garfunkel, E.; Su, D.; Borodin, O.; Wang, C.,  
31 Electrolyte design for LiF-rich solid–electrolyte interfaces to enable high-performance  
32 microsized alloy anodes for batteries. *Nature Energy* **2020**, *5* (5), 386-397.
- 33  
34  
35  
36  
37  
38  
39  
40  
41  
42  
43  
44  
45  
46  
47  
48  
49  
50  
51  
52  
53  
54  
55  
56  
57  
58  
59  
60

The table of contents entry should be 50–60 words long and should be written in the present tense and impersonal style (i.e., avoid we). The text should be different from the abstract text.

**Keyword** surface organic carbonate group, hydrosilylation reaction, Si nanoparticles, solid-electrolyte-interface

## Engineering Si Anode Interface *via* Particle Surface Modification: Embedded Organic Carbonates Lead to Enhanced Performance

Sisi Jiang, Zhenzhen Yang, Yuzi Liu, Noah Johnson, Ira Bloom, Lu Zhang, and Zhengcheng Zhang\*

**ToC figure** ((Please choose one size: 55 mm broad  $\times$  50 mm high **or** 110 mm broad  $\times$  20 mm high. Please do not use any other dimensions))

